Ullah, Kaleem; Liu, Xuefeng; Krasnok, Alex; Habib, Muhammad; Song, Li; García-Cámara, Braulio (2018) Resolving the multipolar scattering modes of a submicron particle using parametric indirect microscopic imaging, *Photonics and Nanostructures - Fundamentals and Applications*, v. 30, pp.: 7-13.

DOI: https://doi.org/10.1016/j.photonics.2018.04.001

Resolving Multipolar Scattering Modes of Submicron Dielectric Particle using Parametric Super Resolution Method

Kaleem Ullah[1], Xuefeng Liu[1,*], Alexander Krasnok[2], Muhammad Habib[3], Li Song[3] and Braulio Garcia-Camara[4]

[1]School of Electronic Engineering and Optoelectronics Technology, Nanjing University of Science and Technology, 200 Xiaolingwei, 210094, People's Republic of China.

[2]Department of Electrical and Computer Engineering, University of Texas at Austin, Austin, Texas 78712, USA.

[3]National Synchrotron Radiation Laboratory, CAS Center for Excellence in Nanoscience, University of Science and Technology of China, Hefei, Anhui, 230029, People's Republic of China.

[4]Group of Displays and Photonic Applications (GDAF-UC3M). Carlos III University of Madrid. Leganes, 28911 Madrid, Spain.

* liuxf1956@163.com

Abstract

In this work, we show the spatial distribution of the scattered electromagnetic field of dielectric particles by using a new super-resolution method based on polarization modulation. Applying this technique, we were able to resolve the multipolar distribution of Cu_2O particles with a radius of 450 nm. In addition, FDTD and Mie simulations have been carried out to validate and confirm the experimental results. The results are helpful to understand the resonant modes of dielectric submicron particles which have a broad range of potential applications, such as all-optical devices or nanoantennas.

Keywords: Polarization modulation, scattering, resonant modes.

Introduction

High-permittivity dielectric materials, such as silicon, are widely used in micro and nano-electronics due to their electric properties, and compatibility with CMOS techniques. Also, they

are important in the design of optical components, such as nano-antennas [1]. Their low losses in the visible and near-infrared ranges, as well as their capacity to support either electric or magnetic Mie resonances make them unique in the control of light scattering [2]. Directional light scattering has been reported in dielectric nanoparticles, including spherical [3–5] and cylindrical [6,7] structures. These features make dielectric nanoparticles an alternative to plasmonic ones [8,9]. In this sense, they can potentially be the basic element of upcoming all-optical devices in a wide range of applications, ranging from bio-sensing [10] to new communication devices [11,12]. Thus, the interest on light scattering of dielectric nanoparticles has strongly increased in the last years [13–16]. The fabrication of silicon is not trivial because of the difficulty in controlling the shape of the particles [39]. Several works have been reported on other high refractive index materials which support Mie resonances such as Germanium (Ge), gallium arsenide (GaAs), Indium Phosphide (InP) etc. [40]. In this work, we analyze the scattering properties of sub-micron particle made of copper (I) oxide (Cu_2O), whose optical properties are adequate to support Mie scattering resonances in the visible region [41]. This material provides us a better control in fabricating different shaped nanostructures as compared to silicon [38] and already has potential applications in solar energy conversion, catalysis and gas sensors, which may be improved with the emergence of these resonances, enlarging its applicability [39].

The first theoretical and experimental demonstration about the electric and magnetic dipolar resonance from silicon nanoparticle in the visible range was reported [17,18]. Several studies about electric and magnetic resonance in dielectric nanoparticles can be found in the literature [19–23]. Both near- and far-field scattering properties are worthy of investigating due to their importance in the interactions with adjacent structures and their practical implementation, respectively. The far-field analysis is usually performed by dark-field spectroscopy [24]. However, the imaging technique is also quite interesting. Unfortunately, the resolution of conventional optical microscopy is constrained by the diffraction limit and thus cannot resolve the sub-wavelength features of the sample under test (SUT) in the far field region. The information about small features of the SUT is included in the evanescent waves, which decay exponentially with distance and are detectable only in the near field region. In the far field region, the loss of these evanescent waves and the information that they contain precludes reconstructing an image of an object with a resolution better than one-half of the incident wavelength [25].

While commonly used dielectric nanoparticles have simple shapes, their arrangements may have sub-wavelength details, like hot-spots in dimer structures [26]. Super-resolution far-field method is deserved to be explored and it is full of challenges. Many super-resolution far-field imaging techniques are based on fluorescence, few non-fluorescent species based far-field imaging can achieve super-resolution [27]. However, these standard far-field techniques offer limited information about subwavelength scattering signal distribution in the far field region especially about the high-order multipolar modes, which provides new opportunities for directional and complex-polarization controlled emission from nano-emitters [28,29]. In fact, we previously reported a polarization-based method which resolves sub-diffraction details in graphene layers [29]. This technique, which is known as Parametric Indirect Microscopic Imaging (PIMI), resolves sub-diffraction features of the SUT by modulating the optical field, fitting the field intensity variation curves of each pixel of the image and extracts the indirect polarization parameters. The imaging process reduces the width of the point spread function (PSF) by filtering off the irrelevant scattering from neighboring source points with different local structure characteristics in the SUT and leads to break the diffraction limit [29]. In this work, we successfully applied PIMI technique to study the electromagnetic (EM) scattering of copper (I) oxide *(Cu_2O)* particles. In particular, we report the spatial distribution of the scattered localized optical modes of a *Cu_2O* submicron particle. A comparison between experiments and simulations also shows the accuracy of this method to characterize light scattering of high-permittivity dielectric nanoparticles. The successful results of far-field scattering characterization, even when magnetic modes arise, show that PIMI is a powerful tool to perform future super-resolution imaging of complex arrangements of dielectric resonant nanoparticles.

Theoretical and Experimental Basis

Before impinging on the SUT, the polarization status of the incoming light is modulated in a controlled and precise manner in PIMI. The linearly polarized light with different polarization angles as shown in Fig. 1(b) excite different scattering information due to the anisotropy present in the SUT. This anisotropy produces near to far field coupling. When this light comes to the CCD after the interaction with the SUT, it can be formulated with the Jones model [43] and also we can check whether the derived intensity follows the near to far field coupling principle or not [29]. The spatial points which follow the coupling principle fit well with the fitting criteria such as adjusted-

root-square (Adj-R-Square) [29], whereas the others do not follow filtered off as noise. Only the middle portion of the pixel intensity confirms the near to far field coupling and the remaining spatial field points filter off. In this way, the width of the PSF decreases and we become able to sense the scattering signals beyond the diffraction limit. The Fig. 1(a) shows the fitting curve fitting the experimental data points.

In Fig. 1(b), a schematic of the polarization illumination has been shown and Fig. 1(c-h) shows the recorded scattered field of a Cu_2O sphere under the different polarization illuminations. As it can be seen in Fig. 1(c-h), at every different polarization illumination, we get different scattered field distribution and then by using our re-construction method, we fit every data point as shown in Fig. 1(a) and extracts fine information about the scattering field. Due to this extra scattering sensing, PIMI makes us enable to study the angular scattering distribution of the scatterer in a much better way. By using the anisotropy, $sin\delta$, which is the phase shift between the phase of the two electric field components, Ey and Ex [30], the azimuthal angle or the slow vibration angle, the angle along the slow vibrational axis [43] and I_{dp}, we calculated the Stokes parameters. I_{dp} is the average of all polarization scattered from the SUT. This means that if, for instance, we rotated the linear polarization field with an angle step of 36° i.e. 0°, 36°, 72°, so on, I_{dp} is the average of all scattering field information of these polarizations [43]. By using a relationship between the Jones and Muller models, we previously introduced a model to calculate the Stokes parameter [29].

$$
\begin{aligned}
S_0 &= I_{dp}(1+\sin\delta) = E_{0x}^2 + E_{0y}^2 \\
S_1 &= I_{dp}(1+\sin\delta)\cos 2\phi = E_{0x}^2 - E_{0y}^2 \\
S_2 &= 2\sqrt{I_{dp}}(1+\sin\delta)\cos 2\phi = 2E_{0x}E_{0y}\sin\delta \\
S_3 &= 2\sqrt{I_{dp}}(1+\sin\delta)\sin 2\phi = 2E_{0x}E_{0y}\cos\delta
\end{aligned}
\qquad (1)
$$

Where E_{0x} and E_{0y} are the amplitude of the electric field on the x and y-axis [30], respectively, which can be derived from our experimental data using equation (1). The PIMI parameters not just provide us the information about the scattering distribution around the scatterer, instead, they delivered the information about the polarization states, polarization degree, and polarization angle.

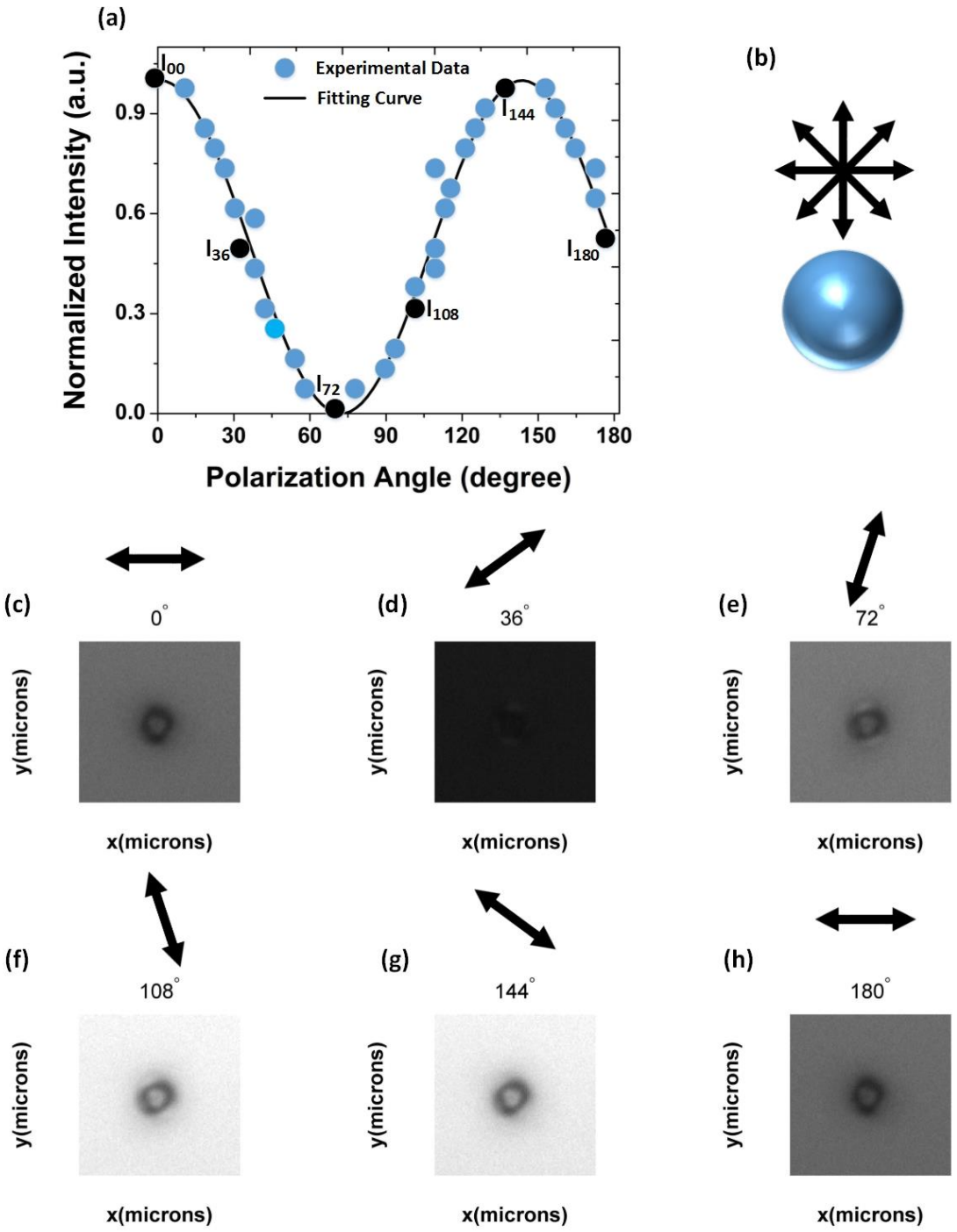

Figure 1. (a) A representation of the experimental scattering data points and their fitting curve for one pixel on the CCD for a polarization angle range of 0º to 360º (b) Schematic of the interaction of modulated field with the SUT. (c-h) The bright field images of the scattering field around a Cu_2O spherical particle at 532 nm wavelength obtained by using 100x objective of numerical aperture under different polarization illumination.

Results and Discussion

An experimental setup of the PIMI system has been displayed in Fig. 2(a) whose details are present in the method section. The considered particles are made of copper (I) oxide (Cu_2O), a dielectric material with a relative high-refractive index (3.22+.033i) at 532 nm [41] to support Mie modes [1-3] and with low losses in the visible and near-IR range [31]. Crystalline Cu_2O nanoparticles were deposited on a silicon (Si) substrate and characterized through SEM (Scanning Electron Microscope) images. A scanning electron micrograph of a Cu_2O particle is shown in Fig. 2(b). It can be seen that it has a well-defined spherical shape and it has an average radius of 450 nm. This particle size allows a simple and more accurate fabrication than using sub-wavelength particles as well as the excitation of several multipolar modes at the considered wavelength. The probed operation of the method in sub-diffraction structures [30] enables to assume that it can also be used in the characterization of a nanoparticle.

Mie calculations were performed to investigate the optical response of these particles and, in particular, the multipolar contributions. Figure 3(a) shows both the scattering and absorption efficiencies of isolated Cu_2O particles with a radius of 450 nm as a function of the incident wavelength calculated by Mie theory [32]. At the wavelength of interest (solid line at 532 nm in Fig. 3), the scattering effect is dominant; however, a non-negligible absorption is still presented, which limits the observance of pure scattering phenomena. Fortunately, scattering signals have a strong intensity that could be detected by our experimental set-up. Operation at longer wavelengths enables the dominant scattering behavior and reduces the influence of absorption losses. The different multipolar scattering contributions are displayed in Fig. 3(b). The high radius/wavelength ratio of the considered particle supports several multipolar contributions. It should be mentioned that only the dominant ones in the considered wavelength range are shown in this figure. In particular, electric and magnetic dipolar (ED and MD), quadrupolar (EQ and MQ) and octupolar (EO, MO) contributions are displayed. These modes are directly related to Mie coefficients a_1, b_1, a_2, b_2, a_3, and b_3, respectively [33]. At the considered incident wavelength (532 nm), several modes have significant values. The most important ones are related to an electric quadrupolar mode (a_2) and an octupolar magnetic mode (b_3). In particular, the latter one achieves a maximum value at this wavelength. On the other hand, while the electric and magnetic dipolar modes (a_1 and b_1) cross each other, their effect is mainly exceeded by the previous ones. This will be shown in the following results.

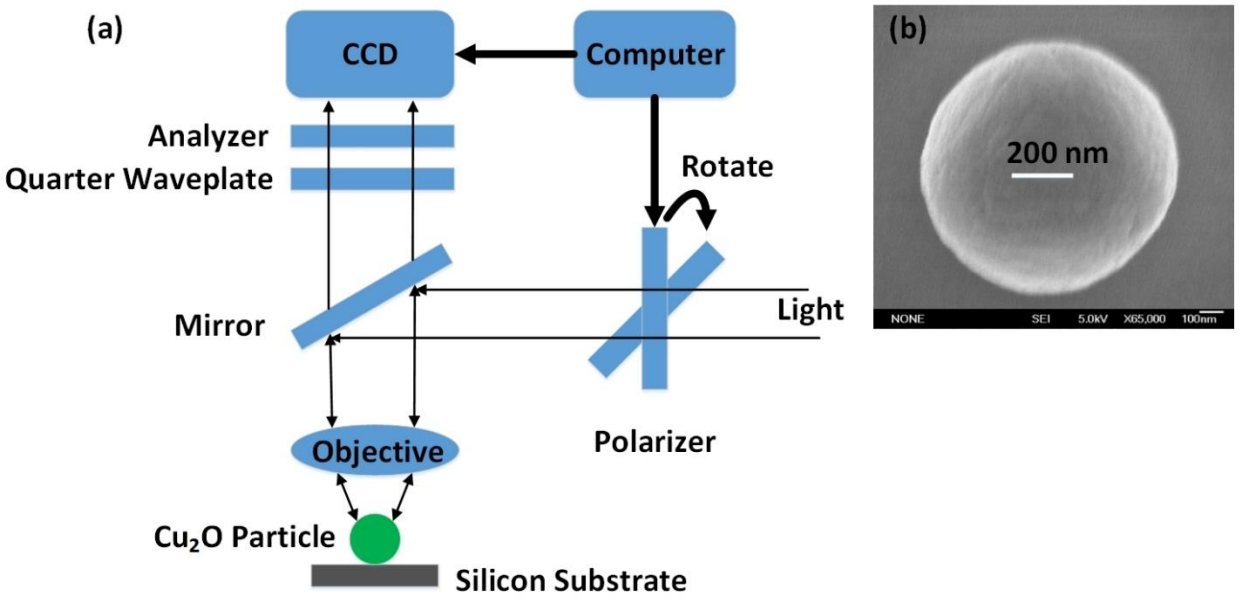

Figure 2. (a) Schematic of a PIMI System (b) SEM measurement of the Cu_2O particle.

Experimental results, obtained through the PIMI technique, are shown in Fig. 4. Fig. 4(a) represents the EM field distribution delivered by the conventional optical microscopy I_{00}. This image shows an isotropic distribution of the scattered field around the particle, as well as an intense concentration in the inner part. This agrees with the fact that these particles can be observed under conventional microscopy due to their resonant response. They seem as bright points. In this figure, it can be seen that the intense radiation from the border of the particle looks like a ring while an intense concentration of light is focused in its center. However, as can be seen in Fig. 2, the multipolar contributions at the target wavelengths should produce a more complex distribution of light in and around these particles.

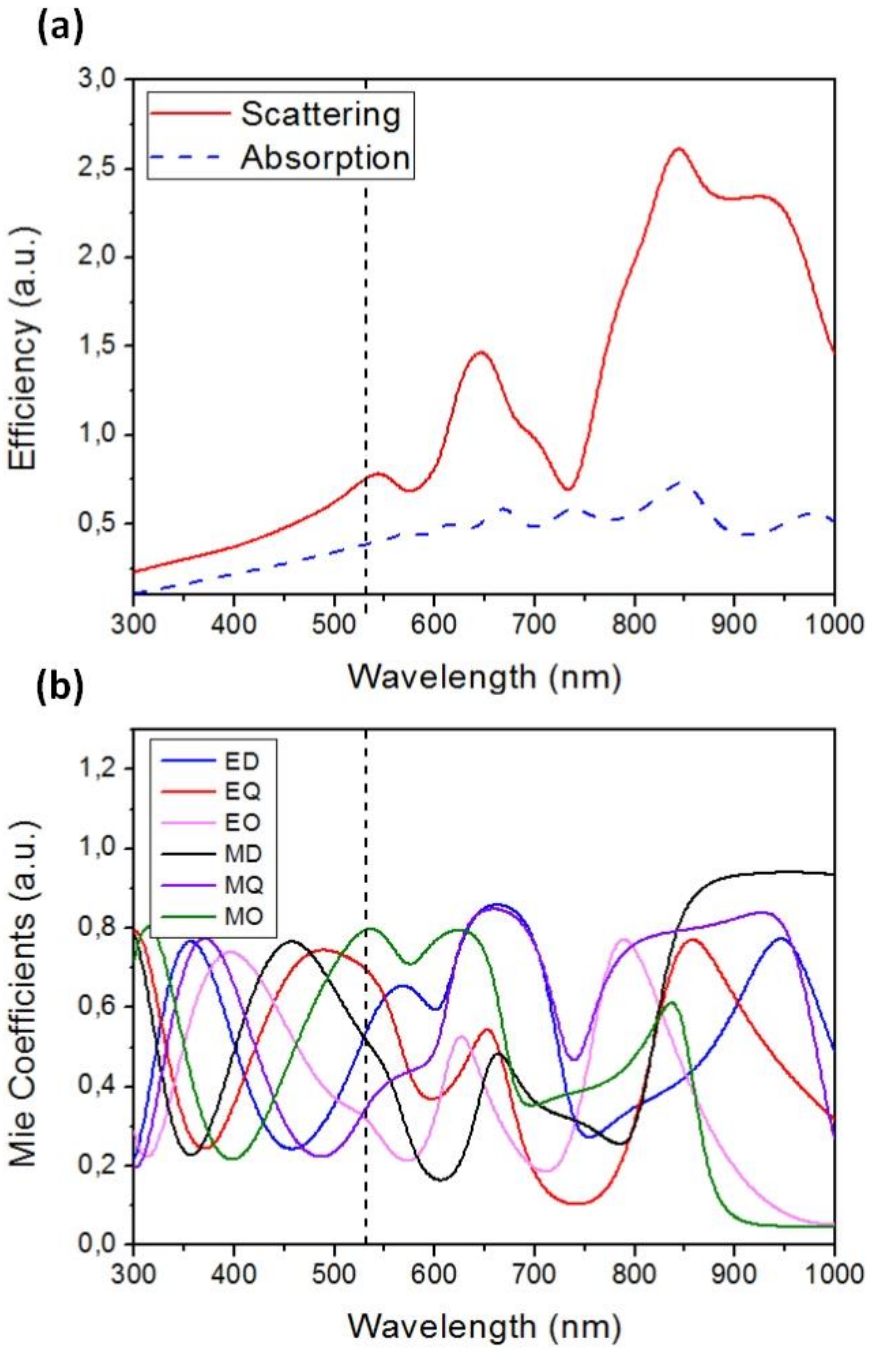

Figure 3. (a) Mie calculations of the scattering (red) and absorption (blue) efficiencies of a Cu_2O particle with a radius of 450 nm as a function of the incident wavelength. (b) First three multipolar contributions, corresponding to dipolar, quadrupolar and hexapolar contributions, including electric and magnetic modes, as a function of the incident wavelength. The vertical dashed (both in "a" and "b") line identifies the incident wavelength in the experiment.

The average of all polarization intensities I_{dp} (Fig. 4b) also shows a similar distribution, although a more spherical shape is observed as compared to the I_{00} and in accordance with SEM images (Fig. 1). Instead, the spatial distribution in $sin\delta$ and ϕ images (Figs. 4c and 4d) shows a more complex profile with a well-defined structure both in and around the particle. This is in accordance with Mie calculations (Fig. 3) Polarization PIMI enables us to detect the azimuthal variation of the spatial scattering distribution much better than the conventional microscopy as clearly can be seen from the Fig. 4. In other words, PIMI technique offers a more detailed information about the scattered field distributions of the resonant dielectric particles than conventional microscopy. Except for I_{dp}, every parameter of the PIMI represents the azimuthal variation of the scattered field in an excellent way. This exception lies in the fact that I_{dp} gives us the average effect of all the polarization and then there is no information about EM lobes.

The excitation of magnetic resonances in natural materials is currently a hot topic in the field of Nanophotonics. The induced magnetism in high-permittivity dielectric nanoparticles can avoid the use of metamaterials to obtain an artificial magnetism [34], simplifying the practical implementation of several applications, e.g. in biomedicine [35], or the excitation of nonlinear effects [36]. Although some of these works are mainly focused on the emergence of the dipolar magnetic contributions, high-order modes are also worthy of exploration. In fact, the interference between dipolar modes allows the observance of directional phenomena [3], the interaction between dipolar and quadrupolar modes produces the excitation of Fano resonances [37]. In this work, the experimental observance and characterization of multipolar modes have been reported. Experimental results show a complex pattern of the scattered field distribution which is a mixture of several multipolar contributions as calculated by the Mie theory at a considered wavelength as shown in Fig. 3b.

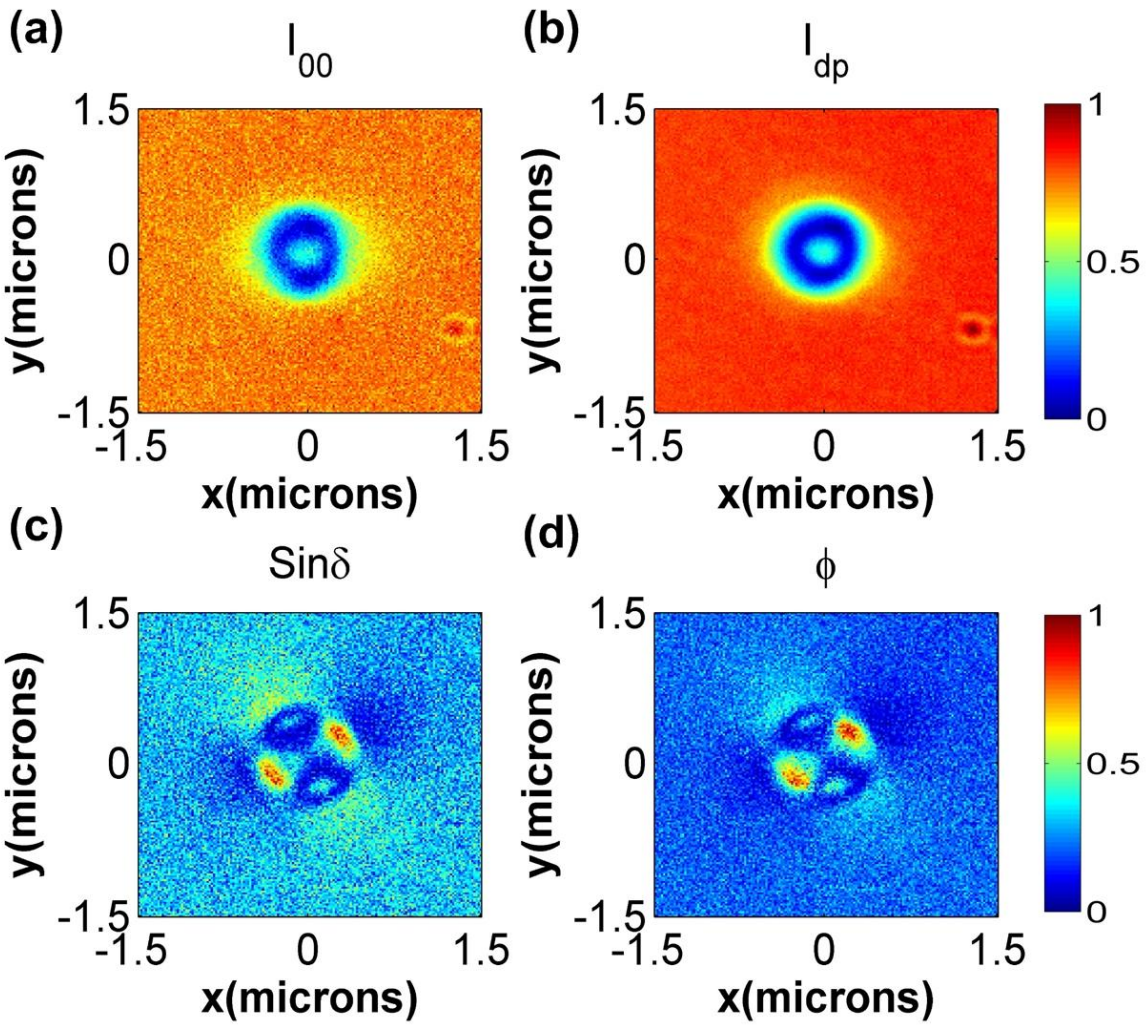

Figure 4. Scattering field distribution delivered by (a) Conventional microscopic Intensity "I_{00}" (b) Average of all polarization intensities "I_{dp}" (c) Phase difference between the orthogonal field components "$sin\delta$" (d) Azimuthal angle or slow vibration angle "ϕ" at 532 nm wavelength.

However, while previous Mie results consider an isolated particle, the substrate of experimental samples can have an important influence [45, 46]. For this reason, FDTD simulations considering a Cu_2O particle with the same size on a silicon substrate are carried out in order to compare with experimental results. Fig. 5 shows both experimental (upper) and numerical (lower panel) spatial distribution of Stokes parameters around the particle. While simulated results show a clear distribution of the Stokes parameters, both in and around the particle, with a large contrast and resolution, experimental ones cannot show it in a similar way. Nonetheless, the profile in the particle can be seen in the experimental measurements. Then, by analyzing the similarity between

both simulated and experimental results, it can be seen that the angular scattering distribution within the boundary of the Cu_2O sphere has a good resemblance to the numerical and experimental images as shown in Fig. 5. The experimental Stokes parameters S_0 and S_1 show a number of maxima and minima and an inner distribution which have been verified by our numerical results. On the other hand, the complexity of the profile in S_3, and the proximity of the two maxima produce that the most important differences appear in this case. Instead of that, the experimental results of S_2 and S_3 are similar and the different details cannot be resolved. Despite this, the results show that PIMI method may solve the spatial distribution of light scattering of resonant dielectric particles in order to identify its dominant character. One of the reasons of small differences found in the scattering profiles of simulated and experimental results is that in simulation, we sliced the particle in a plane, and in the experiment, we could not able to do that. However, the similarity in the S_0 and S_1 simulation and experimental results within the boundary of the particle exists and moreover, the overall scattering pattern of the S_2 and S_3 simulated and experimental results matches. This proves the sensing capability of the PIMI to record the subwavelength scattering modes information in the form of PIMI indirect parameters.

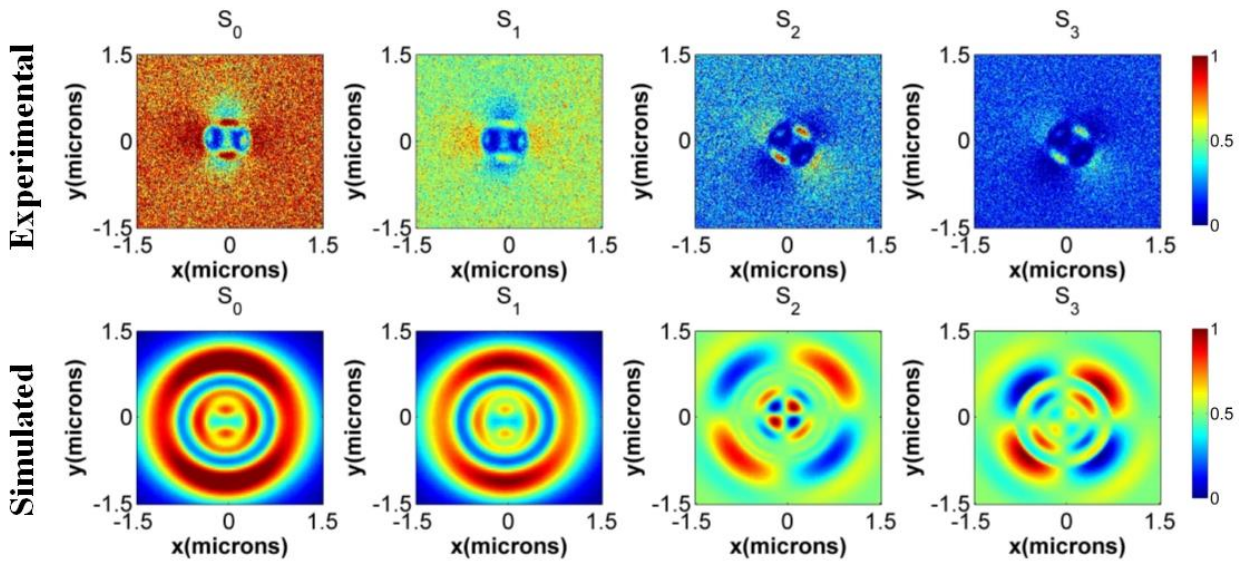

Figure 5. Spatial distributions of the Stokes parameters of a Cu_2O nanoparticle with a radius of 450 nm on a *Si* substrate at a wavelength of 532 nm. Both experimental (upper) and FDTD simulated (lower) results are displayed.

Conclusion

As a summary, we have shown a novel method to resolve the electromagnetic response of high-permittivity dielectric nanoparticles supporting either electric or magnetic multipolar modes. Using polarization parameters, a mapping of light scattering can be detected in the far field, which has been demonstrated numerically and experimentally. In particular, we have displayed the spatial distribution of the localized optical modes of the Cu_2O particle. The azimuthal angle parameter clearly reproduced the profile of light inside the nanoparticles, showing subwavelength light confinement. Apart from the information about the angular distribution of the localized field around the scatterer, PIMI parameters also give us the information about polarization status, polarization degree, and angle.

Methods

Sample Preparation

Crystalline Cu_2O nanoparticles were synthesized by adopting a simple solution method. Reagents used in the synthesis procedure were of research grade (Sigma-Aldrich). For synthesis procedure, first desired molar ratio of PVPMW 30000 (polyvinylpyrrolidone) and $CuCl_2.2H_2O$ (0.01 mol L^{-1}) was achieved by slowly adding PVP into $CuCl_2.2H_2O$ solution drop by drop. NaOH solution (2.0 mol L^{-1}) of an amount of 10ml was mixed into the transparent PVP-$CuCl_2.2H_2O$ solution. The solution was stirred for 30 minutes then 10 ml ascorbic acid (0.6 M) was added to the above solution and then let it aged for 3 hours. Stirring and heating were performed in a water bath. Centrifugation and decanting were performed to get a required precipitate. After washing with deionized water and ethanol precipitate was dried in an oven for several hours. The very detailed experimental conditions are reported by Dong-Feng Zhang et al. [38].

Experimental Setup

The polarization parametric indirect microscopic image (PIMI) system consists of an Olympus reflection microscopic system BX51M which provides the basic optical path. We also incorporated a home-made system in the optical path. This is composed of a polarization modulation module with an angle precision of 0.05 degree and a Basler (PiA2400-17gm) CCD with a pixel resolution of 3.45 micron. The 3.45-micron-pixel CCD resolution leads to an outmost potential resolving power of 34.5nm if diffraction limit is broken and the Nyquist principle is fulfilled in the

microscopic system, working with a 100x objective. The direct and indirect optical images were carried out at the illumination wavelength of 532nm (typical wavelength of the second harmonic of a Nd: YAG laser).

Numerical Simulations

For the verification of our experimental results, we performed the Mie theory and FDTD calculations. Mie theory calculations are performed using the code provided in Ref [32], whereas, for FDTD simulations, we used a plane wave source of wavelength 532 nm according to the experimental setup. To absorb light scattered in all directions, the entire simulation space (a Cu_2O submicron sphere on the silicon substrate) was then surrounded by a perfectly matched layer (PML), whose thickness equals to the half of the working wavelength. The mesh size of 10 nm (length) × 10 nm (width) × 1 nm (height) used for the silicon substrate, whereas, for the particle, it was equal to 25 nm. We confirmed all the field components decayed to zero when the simulation ended, which means that simulation has run sufficiently long time for the Fourier transform to be valid [44].

Acknowledgement

The authors wish to acknowledge the financial support by National Science Foundation China (NSFC) No. 61275163, 61501239, 61605078, 61604073, Natural Science Foundation of Jiangsu Province (Grant No.BK20160839) and the "Zijin Professor Project" of Nanjing University of Science and Technology. MH thanks the National Natural Science Foundation of China for financial support (Project No. U1532112, 11375198, 11574280) and USTC Center for Micro and Nanoscale Research and Fabrication for characterization. MH and KU are grateful to CSC fellowship and Xiaolei Wen for helping with characterization at the Center for Micro and Nanoscale Research and Fabrication.

References

1. Krasnok, A. E., Miroshnichenko, A. E., Belov, P. A. & Kivshar, Y. S. All-Dielectric Optical Nanoantennas. **842,** 837–842 (2012).
2. García-Etxarri, A. *et al.* Strong magnetic response of submicron Silicon particles in the infrared. *Opt. Express* **19,** 4815 (2011).
3. Fu, Y. H., Kuznetsov, A. I., Miroshnichenko, A. E., Yu, Y. F. & Luk'yanchuk, B.

Directional visible light scattering by silicon nanoparticles. *Nat. Commun.* **4,** 1527 (2013).

4. Schmid, M., Andrae, P. & Manley, P. Plasmonic and photonic scattering and near fields of nanoparticles. *Nanoscale Res. Lett.* **9,** 50 (2014).

5. Gómez-Medina, R. Electric and magnetic dipolar response of germanium nanospheres: interference effects, scattering anisotropy, and optical forces. *J. Nanophotonics* **5,** 53512 (2011).

6. Luk'Yanchuk, B. S., Voshchinnikov, N. V., Paniagua-Domínguez, R. & Kuznetsov, A. I. Optimum Forward Light Scattering by Spherical and Spheroidal Dielectric Nanoparticles with High Refractive Index. *ACS Photonics* **2,** 993–999 (2015).

7. Algorri, J. F., Garcia-Camara, B., Cuadrado Conde, A., Sanchez-Pena, J. M. & Vergaz Benito, R. Optimized Minimum-Forward Light Scattering by Dielectric Nanopillars. *IEEE Photonics Technol. Lett.* **28,** 2160–2163 (2016).

8. Kuznetsov, A. I., Miroshnichenko, A. E., Brongersma, M. L., Kivshar, Y. S. & Lukyanchuk, B. Optically resonant dielectric nanostructures. *Science (80-.).* **354,** aag2472-aag2472 (2016).

9. Koenderink, A. F., Alu, A. & Polman, A. Nanophotonics: Shrinking light-based technology. *Science (80-.).* **348,** 516–521 (2015).

10. García-Cámara, B., Gómez-Medina, R., Saenz, Jose, J. & Sepulveda, B. Sensing with magnetic dipolar resonances in semiconductor nanospheres. *Opt. Express* **21,** 23007–23020 (2013).

11. García-Cámara, B. *et al.* All-Optical Nanometric Switch Based on the Directional Scattering of Semiconductor Nanoparticles. *J. Phys. Chem. C* **119,** 19558–19564 (2015).

12. Tribelsky, M. I., Geffrin, J.-M., Litman, A., Eyraud, C. & Moreno, F. Small Dielectric Spheres with High Refractive Index as New Multifunctional Elements for Optical Devices. *Sci. Rep.* **5,** 12288 (2015).

13. Ma, C. R., Yan, J. H., Liu, P., Wei, Y. M. & Yang, G. W. Second harmonic generation from an individual all-dielectric nanoparticle: resonance enhancement versus particle geometry. *J. Mater. Chem. C* **4,** 6063–6069 (2016).

14. van de Groep, J., Coenen, T., Mann, S. A. & Polman, A. Direct imaging of hybridized eigenmodes in coupled silicon nanoparticles. *Optica* **3,** 93 (2016).

15. Fan, P., Yu, Z., Fan, S. & Brongersma, M. L. Optical Fano resonance of an individual semiconductor nanostructure. *Nat. Mater.* **13,** 471–475 (2014).

16. Zhang, X., Wu, T., Zhang, X. & Wang, R. Strongly enhanced Raman optical activity in molecules by magnetic response of nanoparticles. *J. Phys. Chem. C* **120,** 14795–14804 (2016).

17. Evlyukhin, A. B., Reinhardt, C., Seidel, A., Luk'Yanchuk, B. S. & Chichkov, B. N. Optical response features of Si-nanoparticle arrays. *Phys. Rev. B - Condens. Matter Mater. Phys.* **82,** 45404 (2010).

18. Sikdar, D., Cheng, W. & Premaratne, M. Optically resonant magneto-electric cubic nanoantennas for ultra-directional light scattering. *J. Appl. Phys.* **117,** (2015).

19. Terekhov, P. D. *et al.* Multipolar response of nonspherical silicon nanoparticles in the visible and near-infrared spectral ranges. *Phys. Rev. B* **96,** 35443 (2017).

20. Butakov, N. A. & Schuller, J. A. Designing Multipolar Resonances in Dielectric Metamaterials. *Sci. Rep.* **6,** 38487 (2016).

21. Staude, I. *et al.* Tailoring directional scattering through magnetic and electric resonances in subwavelength silicon nanodisks. *ACS Nano* **7,** 7824–7832 (2013).

22. Evlyukhin, A. B. *et al.* Demonstration of magnetic dipole resonances of dielectric nanospheres in the visible region. *Nano Lett.* **12,** 3749–3755 (2012).

23. Kuznetsov, A. I., Miroshnichenko, A. E., Fu, Y. H., Zhang, J. & Luk'yanchuk, B. Magnetic light. *Sci. Rep.* **2,** 492 (2012).

24. Andres-Arroyo, A., Gupta, B., Wang, F., Gooding, J. J. & Reece, P. J. Optical Manipulation and Spectroscopy of Silicon Nanoparticles Exhibiting Dielectric Resonances. *Nano Lett.* **16,** 1903–1910 (2016).

25. Narimanov, E. E. Optical Nanoscope. *Nat. Photonics* **1,** 260–261 (2007).

26. Bakker, R. M. *et al.* Magnetic and electric hotspots with silicon nanodimers. *Nano Lett.* **15,** 2137–2142 (2015).

27. Wang, P. *et al.* Far-field imaging of non-fluorescent species with subdiffraction resolution. *Nat. Photonics* **7,** 449–453 (2013).

28. Habteyes, T. G. *et al.* Near-Field Mapping of Optical Modes on All-Dielectric Silicon Nanodisks. *ACS Photonics* **1,** 794–798 (2014).

29. Liu, X. *et al.* Characterization of graphene layers using super resolution polarization parameter indirect microscopic imaging. *Opt. Express* **22,** 20446 (2014).

30. Collett, E. *Field Guide to Polarization (SPIE Vol. FG05)*.

31. Abu-Zeid, M. E., Rakhshani, A. E., Al-Jassar, A. A. & Youssef, Y. A. Determination of the Thickness and Refractive Index of Cu2O Thin Film Using Thermal and Optical Interferometry. *Phys. status solidi* **93,** 613–620 (1986).

32. Bohren, C. F. & Wiley, J. *Absorption and Scattering of Light by Small Particles*.

33. Liu, W. *et al.* Ultra-directional forward scattering by individual core-shell nanoparticles. *Opt. Express* **22,** 16178 (2014).

34. Markovich, D., Baryshnikova, K., Shalin, A. & Samusev, A. Enhancement of artificial magnetism via resonant bianisotropy. *Nat. Publ. Gr.* 1–8 (2016). doi:10.1038/srep22546

35. Bao, Y. *et al.* Magnetic nanoparticles : material engineering and emerging applications in lithography and biomedicine. *J. Mater. Sci.* (2015). doi:10.1007/s10853-015-9324-2

36. Shcherbakov, M. *et al.* nanoparticles driven by magnetic response Enhanced third-

harmonic generation in silicon nanoparticles driven by magnetic response. (2014). doi:10.1021/nl503029j

37. Bakhti, S. *et al.* Fano-like resonance emerging from magnetic and electric plasmon mode coupling in small arrays of gold particles. *Nat. Publ. Gr.* 1–12 (2016). doi:10.1038/srep32061

38. Zhang, D. F. *et al.* Delicate control of crystallographic facet-oriented Cu2O nanocrystals and the correlated adsorption ability. *J. Mater. Chem.* **19,** 5220–5225 (2009).

39. Zhang, S. *et al.* Colloidal Moderate-Refractive-Index Cu2O Nanospheres as Visible-Region Nanoantennas with Electromagnetic Resonance and Directional Light-Scattering Properties. *Adv. Mater.* **27,** 7432–7439 (2015).

40. García-Cámara, B., Gómez-Medina, R., Saenz, Jose, J. & Sepulveda, B. Sensing with magnetic dipolar resonances in semiconductor nanospheres. *Opt. Express* **21,** 23007–23020 (2013).

41. Malerba, C. *et al.* Absorption coefficient of bulk and thin film Cu2O. *Sol. Energy Mater. Sol. Cells* **95,** 2848–2854 (2011).

42. Ullah, K. *et al.* A Polarization Parametric Method of Sensing the Scattering Signals from a Submicrometer Particle. *IEEE Photonics Technol. Lett.* **29,** 19–22 (2017).

43. Glazer, A. M., Lewis, J. G. & Kaminsky, W. An automatic optical imaging system for birefringent media. *Proc. R. Soc. London Ser. a-Mathematical Phys. Eng. Sci.* **452,** 2751–2765 (1996).

44. Demetriadou, A. The impact of natural modes in plasmonic imaging. *Sci. Rep.* **5,** 1–9 (2015).

45. Kuo, Y. L., Chuang, S. Y., Chen, S. Y. & Chen, K. P. Enhancing the Interaction between High-Refractive Index Nanoparticles and Gold Film Substrates Based on Oblique Incidence Excitation. *ACS Omega* **1,** 613–619 (2016).

46. Sinev, I. *et al.* Polarization control over electric and magnetic dipole resonances of dielectric nanoparticles on metallic films. *Laser Photon. Rev.* **10,** 799–806 (2016).